HEFAT2014
10th International Conference on Heat Transfer, Fluid Mechanics and Thermodynamics
14 - 16 July, 2014, Orlando, Florida
Paper No: 1569879029

LES of Incompressible Turbulent Flow Inside a Cubical Cavity Driven by Two Parallel Lids Moving in Opposite Direction - Effect of Reynolds Number

Devendra Patel, Subhransu Roy and Manab K Das
Department of Mechanical Engineering
IIT Kharagpur, India
Email: suroy@iitkgp.ac.in

Abstract

Large-eddy simulation (LES) of the incompressible turbulent flow in a two-sided lid-driven cubical cavity with lids moving in anti-parallel direction have been carried out at Reynolds numbers of 12000 and 18000 using a computer code developed in-house. Time averaged solutions have been obtained by performing simulations using multi-processing. The presence of multiple eddies other than the well known two corner eddies have been observed in the transverse plane of main core flow direction at both Reynolds number. The specific features of turbulent flow inside the cavity such as some second-order turbulent statistics, turbulent production, dissipation of turbulence have been investigated in the entire domain.
Keywords: LES, Turbulence, Lid-driven cavity

Nomenclature

Roman symbols

C	Smagorinsky coefficient
C^*	Smagorinsky coefficient at previous time step
D	control volume of finite-difference cell
L_{ij}	resolved turbulent stresses
P	modified pressure
t	time
T_{ij}	subtest-scale stresses tensor
U_0	dimensional velocity of centre of moving lid
$U_\tau(x_1, x_2)$	velocity of moving lid
x_i	co-ordinates x, y, z for $i = 1, 2, 3$ receptively
$\overline{f}(\mathbf{x})$	filtering function
$\overline{p}'$	pressure correction
P_t	Turbulent production term
Re	Reynolds number
$\overline{S}_{ij}$	large-scale strain rate tensor for grid-filter
$\widehat{\overline{S}}_{ij}$	large-scale strain rate tensor for test-filter
$\overline{u}_i$	filtered velocities $\overline{u}$, $\overline{v}$, $\overline{w}$ for $i = 1, 2, 3$ receptively
$\overline{u}_i^*$	provisional velocity field

Greek symbols

δ_{ij}	Kronecker's delta
$\langle\varepsilon\rangle$	Average turbulent energy dissipation rate
ν_{sgs}	subgrid-scale eddy-viscosity
$\overrightarrow{\omega}$	vorticity vector
τ_{ij}	subgrid-scale (SGS) stress tensor
τ_{ij}^{turb}	Turbulent shear stress tensor
$\overline{\Delta}$	grid-filter width
$\overline{\Delta}_1, \overline{\Delta}_2$ and $\overline{\Delta}_3$	mesh spacing for grid-filter in x, y and z direction respectively

$\widehat{\overline{\Delta}}$ test-filter width

$\widehat{\overline{\Delta}}_1$, $\widehat{\overline{\Delta}}_2$ and $\widehat{\overline{\Delta}}_3$ mesh spacing for test-filter in x, y and z direction respectively

ω_i Magnitude of vorticity ω_x, ω_y, ω_z for i=1, 2, 3.

Please note that all variables listed above are dimensionless unless stated otherwise.

INTRODUCTION

In the field of incompressible fluid flow research, lid driven cavity is commonly used as a benchmark problem because in spite of its small domain size and simplicity of geometry, the flow inside the cavity offers many complexities like recirculation, turbulence, eddies, instability, impingement, flow separation, attachment with walls (moving and stationary both), fluid trapping inside the recirculation region and many other fluid flow phenomena. These reasons make the study of lid driven cavity important for fluid flow research and development of industrial applications (Shankar and Deshpande [1]).

A large number of experimental and numerical studies on lid driven cavity flows for variety of configurations are present in literature. Shankar and Deshpande [1] have presented an introductory brief literature survey on the study of driven cavity flow upto year 2000.

LES, simulation of the three dimensional flow in one-sided lid-driven cavity were carried out by Bouffanais et al. [2] and others for Reynolds number upto 10000. DNS simulation of the three dimensional flow in lid-driven cavity were carried out by Leriche and Gavrilakis [3] upto Reynolds number of 12000, and recently by Leriche [4], at very high Reynolds numbers upto 22000. In the literature there are very few studies for three-dimensional multiple lid moving situations like Ben Beya and Lili [5], and Oueslati et al. [6] who studied the recirculating flow in an unheated cavity.

In the present days, the Large Eddy Simulation (LES) has become an established technique for the study of turbulent and transitional flows, where large energy carrying eddies are computed accurately, whereas smaller, more universal, nearly homogeneous and isotropic eddies are modeled, making LES more accurate than Reynolds-averaged Navier-Stokes (RANS) approach. The grid size required for LES should be small enough compared to the integral scale of motion, but need not match the very small Kolmogorov scales, which makes LES significantly computationally cheaper than Direct Numerical Simulation (DNS) and applicable to complex turbulent flows at higher Reynolds number and for larger domain size than those achievable by DNS. Recently Large Eddy Simulation of incompressible flow inside a single lid driven cavity have been presented by Bouffanais et al. [2] at Reynolds number 12000 by using both Dynamic Smagorinsky Model (DSM) and Dynamic Mixed Model (DMM).

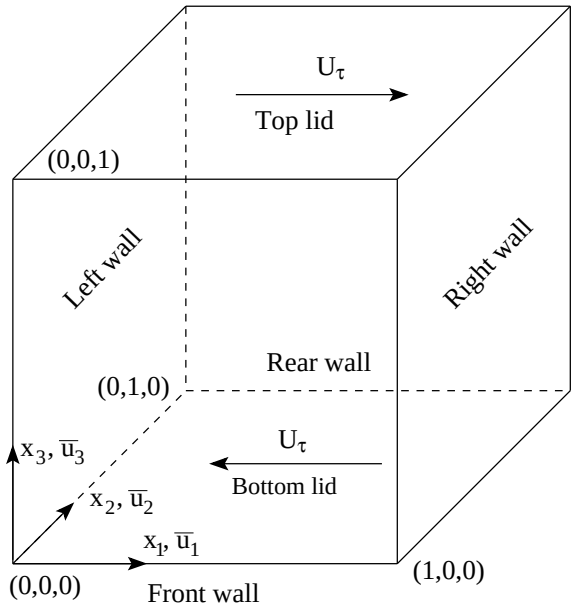

Figure 1: Schematic diagram of cubic cavity driven by two parallel lids moving in opposite direction

In the present paper, two sided cubic lid-driven cavity with lids moving in anti-parallel direction has been studied numerically at 12000 and 18,000 Reynolds number. The mathematical formulation is based on Large Eddy Simulation with Dynamic Smagorinsky Model (LES-DSM) and Filtered Navier-Stokes Equations were discretized using finite difference method. As there were no numerical and experimental results found for comparison in literature, the present code have been validated by Patel et al. [7] with one sided lid-driven cavity flow results obtained by Bouffanais et al. [2] and Leriche and Gavrilakis [3] at Reynolds number 12000 .

MATHEMATICAL FORMULATION

The domain of computation shown in Fig. 1 where the top lid and bottom lid are moving in opposite directions. In

LES the filtered variables or large scale variables (denoted by over-bar) are defined as

$$\overline{f}(\mathbf{x}) = \frac{1}{\overline{\Delta}_1\overline{\Delta}_2\overline{\Delta}_3}\int_D f(x')d\mathbf{x}', \tag{1}$$

using a simple top-hat filter in real space. The filtered Navier-Stokes and the continuity equations for an incompressible flow inside the cavity can be obtained by applying the filtering function (Eq. 1) to the Navier-Stokes and continuity equations. The dimensionless form of the filtered Navier-Stokes and the continuity equations are obtained by using the length of the side of the cavity as characteristic length and the velocity at the center of the moving lid as characteristic velocity. They assume the following dimensionless form:

$$\frac{\partial\overline{u}_i}{\partial t} + \frac{\partial}{\partial x_j}\left(\overline{u}_i\overline{u}_j\right) = -\frac{\partial P}{\partial x_i} + \frac{1}{\mathrm{Re}}\frac{\partial^2\overline{u}_i}{\partial x_j\partial x_j} - \frac{\partial\tau_{ij}}{\partial x_j}, \tag{2}$$

$$\frac{\partial\overline{u}_i}{\partial x_i} = 0, \tag{3}$$

The Reynolds number is defined based on the laminar kinematic viscosity.

Some care is needed in applying the boundary condition at the moving lid. In the present computation, to avoid discontinuity in velocity distribution near the edge of moving lid, a 36 order polynomial velocity distribution $U_\tau(x_1,x_2)$ is chosen as mentioned by Leriche and Gavrilakis [3].

$$U_\tau(x_1,x_2) = \left[1-(2\times(0.5-x_1))^{18}\right]^2\left[1-(2\times(0.5-x_2))^{18}\right]^2$$

$$\left.\begin{aligned}\overline{u}_1(x_1,x_2,1) &= U_\tau(x_1,x_2),\\ \overline{u}_2(x_1,x_2,1) &= \overline{u}_3(x_1,x_2,1) = 0\end{aligned}\right\}\text{for top lid,} \tag{4}$$

$$\left.\begin{aligned}\overline{u}_1(x_1,x_2,0) &= -U_\tau(x_1,x_2)\\ \overline{u}_2(x_1,x_2,0) &= \overline{u}_3(x_1,x_2,0) = 0\end{aligned}\right\}\text{for bottom lid.} \tag{5}$$

The effect of small scales appears in the last term of the Eq. 2 through a sub-grid scale (SGS) stress tensor τ_{ij}. In LES the grid size $\bar{\Delta}$ for filtering is chosen carefully so as to be able to calculate the SGS stress tensor given by $\tau_{ij} = \overline{u_iu_j} - \overline{u}_i\overline{u}_j$ correctly. SGS stress tensor is connected to the large-scale strain rate tensor $\overline{S}_{ij}$ by an subgrid-scale eddy viscosity (ν_{sgs}) parameter modeled by Smagorinsky [8] as

$$\tau_{ij} - \frac{\delta_{ij}}{3}\tau_{kk} = -2\nu_{sgs}\overline{S}_{ij} = -2\left(C_s\overline{\Delta}\right)^2\left|\overline{S}\right|\overline{S}_{ij} = -2C\beta_{ij} \tag{6}$$

where,

$$\beta_{ij} = \overline{\Delta}^2\left|\overline{S}\right|\overline{S}_{ij} \tag{7}$$

$$\overline{S}_{ij} = \frac{1}{2}\left(\frac{\partial\overline{u}_i}{\partial x_j} + \frac{\partial\overline{u}_j}{\partial x_i}\right) \tag{8}$$

$$\overline{\Delta} = \left(\overline{\Delta}_1\overline{\Delta}_2\overline{\Delta}_3\right)^{\frac{1}{3}} \tag{9}$$

and $\left|\overline{S}\right| = \left(2\overline{S}_{i,j}\overline{S}_{i,j}\right)^{\frac{1}{2}}$ is the magnitude of the large-scale strain rate tensor. Germano et al. [9] and Lilly [10] introduced a method to calculate C in Eq. 6 for each time step and grid point dynamically from the flow field data. If the test filter of size $\widehat{\overline{\Delta}}$ (at least twice that of grid filter $\overline{\Delta}$) is applied to the governing equations (Eq. 2 and Eq. 3), a new set of stress appear called subtest-scale stresses, T_{ij}, in the filtered Navier-Stokes equations

$$\frac{\partial\widehat{\overline{u}}_i}{\partial t} + \frac{\partial}{\partial x_j}\left(\widehat{\overline{u}}_i\widehat{\overline{u}}_j\right) = -\frac{\partial\widehat{P}}{\partial x_i} + \frac{1}{\mathrm{Re}}\frac{\partial^2\widehat{\overline{u}}_i}{\partial x_j\partial x_j} - \frac{\partial T_{ij}}{\partial x_j},$$

$T_{ij} = \widehat{\overline{u_iu_j}} - \widehat{\overline{u}}_i\widehat{\overline{u}}_j$ can be parametrized by the same eddy viscosity model of Smagorinsky [8] as shown below.

$$T_{ij} - \frac{\delta_{ij}}{3}T_{kk} = -2\left(C_s\widehat{\overline{\Delta}}\right)^2\left|\widehat{\overline{S}}\right|\widehat{\overline{S}}_{ij} = -2C\alpha_{ij} \tag{10}$$

where,

$$\alpha_{ij} = \widehat{\overline{\Delta}}^2\left|\widehat{\overline{S}}\right|\widehat{\overline{S}}_{ij} \tag{11}$$

$$\widehat{\overline{S}}_{ij} = \frac{1}{2}\left(\frac{\partial\widehat{\overline{u}}_i}{\partial x_j} + \frac{\partial\widehat{\overline{u}}_j}{\partial x_i}\right), \tag{12}$$

$$\widehat{\overline{\Delta}} = \left(\widehat{\overline{\Delta}}_1\widehat{\overline{\Delta}}_2\widehat{\overline{\Delta}}_3\right)^{\frac{1}{3}}, \tag{13}$$

$$\frac{\widehat{\overline{\Delta}}}{\overline{\Delta}} \geq 2 \tag{14}$$

The consistency between equations (Eq. 6 and Eq. 10) depends on the proper choice of C [9], which can be achieved by subtraction of the average subgrid-scale stress $\widehat{\tau}_{ij}$ from subtest-scale stress T_{ij} as suggested by Lilly [10] and Hoffmann and Benocci [11].

$$L_{ij} = T_{ij} - \widehat{\tau}_{ij} = -2C\alpha_{ij} + 2\widehat{C\beta_{ij}} \tag{15}$$

where, L_{ij} is resolved turbulent stress given by

$$L_{ij} = \widehat{\overline{u_iu_j}} - \widehat{\overline{u}}_i\widehat{\overline{u}}_j \tag{16}$$

NUMERICAL SCHEME AND METHOD OF SOLUTION

To discretize the governing equations a three-dimensional staggered finite-difference grid is adopted where the scalar variables are located in the main grid points and the dimensionless filtered velocity variables $\overline{u}$ $\overline{v}$ and $\overline{w}$ are staggered in the x y and z directions respectively and located at the center of the main scalar grid points. The hyperbolic tangent transformation is used to get dense grid cells near the wall and coarse grid cells in the center of cavity. In the governing equations (Eq. 2 and Eq. 3), all spatial derivatives are approximated by second order central differences scheme on staggered grid. A second order time-accurate explicit Adams–Bashforth fractional-step method was used for time integral; other terms (advective and diffusive) were treated explicitly. In LES computation the grid size for filtering and the time step are carefully chosen as in Patel et al. [7]. The number of grid points in the present computation is $(71 \times 71 \times 71 = 357911)$. To be in safer side, the non-dimensional time step taken is 0.001 which is less than that obtained by CFL condition.

The solution of pressure correction equation (Eq. 17) ensures mass continuity.

$$\frac{\partial^2 \overline{p}'}{\partial x_i^2} = \frac{2}{\triangle t} \frac{\partial \overline{u}_i^*}{\partial x_i} \tag{17}$$

Here $\overline{u}_i^*$ is the intermediate velocity field obtained from the momentum equation for the uncorrected pressure field. Conjugate gradient method is used to solve the pressure correction equation (Poisson's Eq. 17) iteratively.

A simpler iterative procedure suggested by Piomelli and Liu [12], based on the modification of equation (Eq. 15), is used to get the value of Smagorinsky coefficient C locally (Eq. 18) for each time step and scalar grid point.

$$C(x, y, z, t) = -\frac{1}{2} \frac{\left(L_{ij} - 2\widehat{C^* \beta_{ij}}\right) \alpha_{ij}}{\alpha_{mn} \alpha_{mn}} \tag{18}$$

Whenever the value of the coefficient C was negative, the lower limit was set to zero and the upper limit was set to 0.18^2 to maintain the numerical stability. The computations are considered to be converged when residuals for the equations (Eq. 17 and Eq. 18) are below 1×10^{-6} in each time step.

As the time steps are very small and the number of grids very large the computation time is very long; so it requires multiprocessing. In the present computation 12 number of processors have been used. Due to the large number of grid points and the small time steps the converged results of different variables are stored after every 500 time steps corresponding to a dimensionless time interval of 0.5 for further analysis. The computer results were validated by Patel et al. [7] for the cubic lid-driven cavity with top lid moving towards positive x-direction.

RESULTS AND DISCUSSION

The flow inside a cavity with two opposite lids moving in opposite directions produces a strong recirculating core flow in the center region with secondary recirculation at the corners. This type of motion at high Reynolds number gives rise to turbulent fluctuations. The turbulent transient characteristics of the flow at Reynolds numbers 12000 and 18000 have been captured by calculating the value of the flow field variable inside the domain at dimensionless time steps of 0.001.

The ensemble average is taken for whole dynamic range up to the end of the simulation to get the time averaged flow field data. The fluctuating component of any variable is calculated using Reynolds statistical splitting such that $\overline{a} = \langle \overline{a} \rangle + \overline{a}'$, where, $\overline{a}$ =instantaneous value, $\langle \overline{a} \rangle$ =average value, and $\overline{a}'$ =fluctuating part. Here $\overline{a}'$ represent the large scale fluctuations which are computed.

The various mean flow and turbulent fluctuation features of the two-lid-driven cavity are presented in the following sub-sections.

Flow Characteristics In The Plane Of Statistical Symmetry ($y = 0.5$)

The recirculating flow in the lid-driven cavity is mainly taking place in the $x-z$ plane. The fluid driven by the top lid moving in x-direction impinges into the right-side vertical wall and the flow continues to develop in the downward direction like a wall jet. This fluid then driven by the bottom lid moving in the $(-)x$-direction, impinges into the left-side vertical wall and develops like a wall jet in the upward direction. Fig. 2 shows the average velocity vector plot at the mid plane $y = 0.5$; here a vertical wall jet type velocity profile near to the left-side and right-side vertical wall is visible.

The fluid driven horizontally by the moving lids at the top and bottom impinges on the solid vertical walls and changes its direction along the vertical wall. This sharp

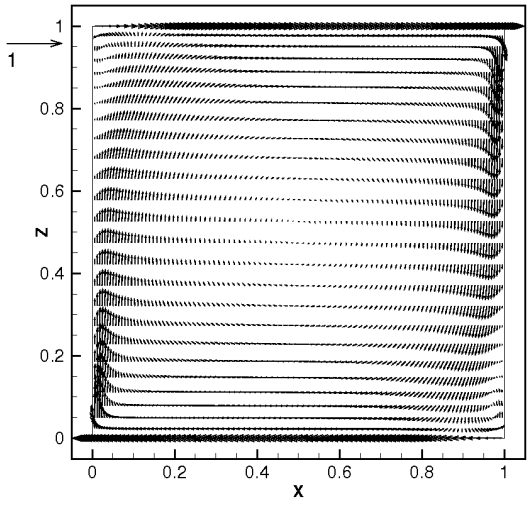

Figure 2: Averaged velocity vectors at the statistical symmetry plane ($y = 0.5$) at Re=18000.

turn dissipates large amounts of energy, which results in increase of pressure in that corner region where the wall jet originates. On closer examination of Fig. 2 we see that the wall jets decelerate on its way and finally separate from the wall due to adverse pressure gradient on reaching the corner at the end of its travel and form two corner eddies, one in the region near to the bottom side of right-side vertical wall and another in the region near to the top side of left-side vertical wall. These two corner eddies of almost same size are rotating in opposite directions. The velocity vectors for Re=18000 are shown in Fig. 2. The flow at Re=12000 shows similar flow behavior but the magnitude of the velocity throughout the domain decrease and the size of the corner eddies increases with lower Reynolds number. For the sake of simplicity, the term "first corner eddy" will be used for the corner eddy which is in the region near to the bottom side of right-side wall and "second corner eddy" will be used for the corner eddy which is in the region near to the top side of left-side wall.

Figures 3 and 4 show the contour plot of the RMS values of large scale fluctuating velocity component $\sqrt{\langle \overline{u}'^2 \rangle}$ and $\sqrt{\langle \overline{w}'^2 \rangle}$ at the mid-plane $y = 0.5$ at Re of 12000 and 18000. These profiles are almost antisymmetric in nature. The large scale fluctuations in the velocity components very near to the walls and in the central core regions, are extremely low. According to Fig. 3 RMS value $\sqrt{\langle \overline{u}'^2 \rangle}$ reaches its maximum range of 0.09 at the edge of the boundary layer at the top and bottom moving lid; and

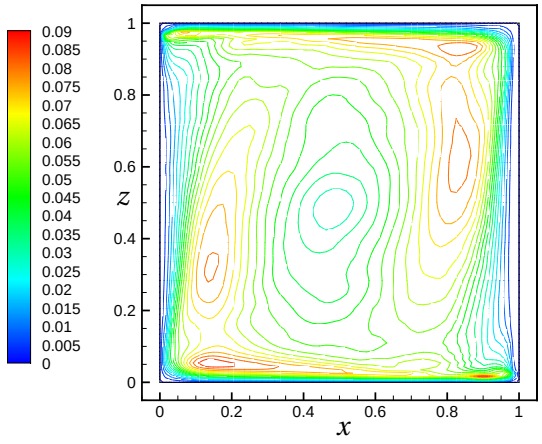

(a) Re = 12000. (In the domain $0 \le \sqrt{\langle \overline{u}'^2 \rangle} \le 0.134$) [13]

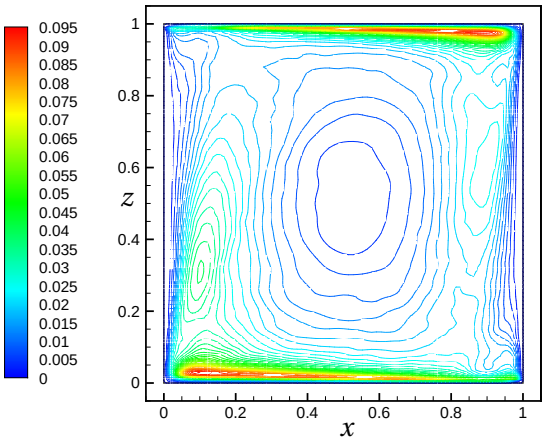

(b) Re = 18000 (In the domain $0 \le \sqrt{\langle \overline{u}'^2 \rangle} \le 0.125$)

Figure 3: The comparison of second-order turbulent statistics $\sqrt{\langle \overline{u}'^2 \rangle}$ at statistical symmetry plane ($y = 0.5$).

it also reaches a high value of 0.08 at the edge of the vertical wall jet for Re = 12000. For Re = 18000 the RMS value $\sqrt{\langle \overline{u}'^2 \rangle}$ reaches a high value of 0.095 at the edge of the boundary layer at the top and bottom moving lid; and it also reaches a high value of 0.05 at the edge of the vertical wall jet. According to Fig. 4 the RMS value $\sqrt{\langle \overline{w}'^2 \rangle}$ reaches a high value of 0.15 for Re = 12000 and a high value of 0.18 for Re = 18000 at the edge of the vertical wall jet. The Fig. 5 shows contour plot of the dominating component $\langle \overline{u}'\overline{w}' \rangle$ of the large scale Reynolds stress in statistical symmetry plane $y = 0.5$. The value of this Reynolds stress component reaches a high value of 0.008 at Re = 12000 and a high value of 0.052 at Re = 18000 near the edge of the vertical wall jet. This Reynolds stress component also reaches a

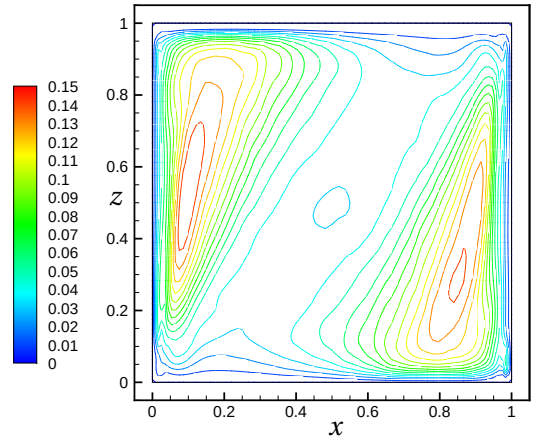

(a) Re = 12000 (In the domain $0 \le \sqrt{\langle \overline{w}'^2 \rangle} \le 0.15$) [13]

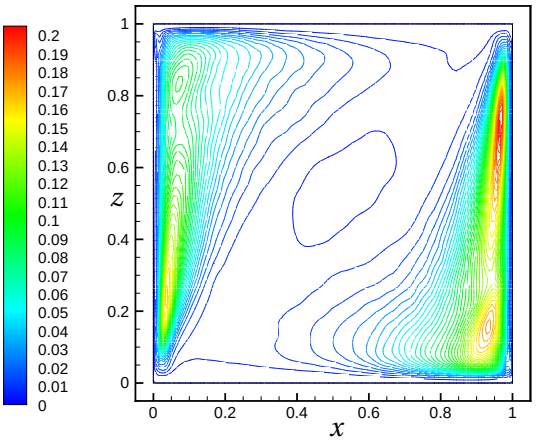

(b) Re = 18000 (In the domain $0 \le \sqrt{\langle \overline{w}'^2 \rangle} \le 0.238$)

Figure 4: The comparison of second-order turbulent statistics $\sqrt{\langle \overline{w}'^2 \rangle}$ at statistical symmetry plane ($y = 0.5$).

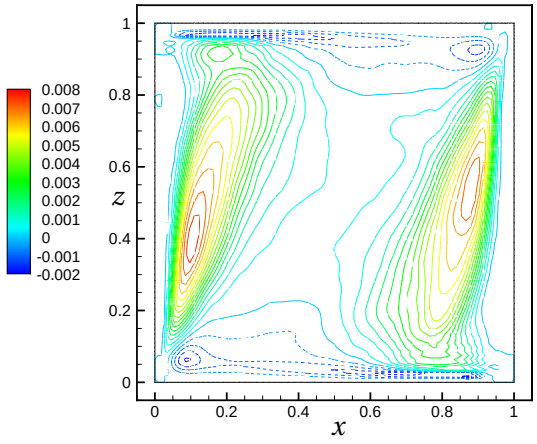

(a) Re = 12000. (In the domain $-3.5 \times 10^{-3} \le \langle \overline{u}'\overline{w}' \rangle \le 1.05 \times 10^{-2}$)[13]

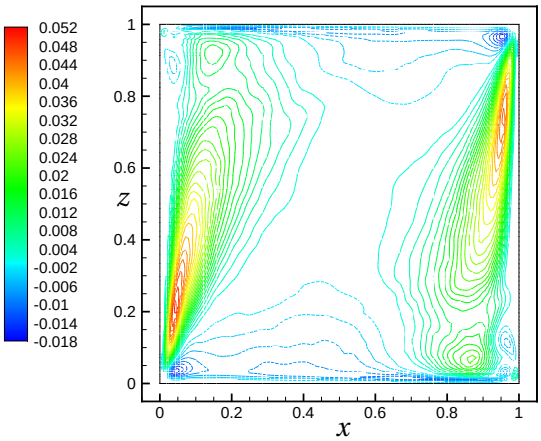

(b) Re = 18000. (In the domain $-2.3 \times 10^{-3} \le \langle \overline{u}'\overline{w}' \rangle \le 6.0 \times 10^{-2}$)

Figure 5: The comparison of second-order turbulent statistics $\langle \overline{u}'\overline{w}' \rangle$ at statistical symmetry plane ($y = 0.5$).

high negative value of -0.002 for Re = 12000 and a high negative value of -0.018 in the inner part of the boundary layer at the top and bottom moving lid. Here negative contour levels are shown as dashed lines. The contour plots show that the dominating component $\langle \overline{u}'\overline{w}' \rangle$ of large scale Reynolds stress is having maximum magnitude in regions where maximum shear flow occurs and the flow is highly turbulent. It is also observed that in the central core region the large scale turbulent fluctuating component of velocity is very low and the large scale turbulent Reynolds stress is very small.

The turbulent production term P_t is defined as

$$P_t = -\overline{u}_i'\overline{u}_j' \frac{\partial \langle \overline{u}_i \rangle}{\partial x_j} \tag{19}$$

which can be interpreted as responsible for the production of turbulence.

In Fig 6 the turbulent production $\langle P_t \rangle$ in the cavity varies in the range of -0.014 to 0.12, but in the statistical symmetry plane the maximum value in the range of 0.03 to 0.036 occurs near the four corners for Re = 12000. For Re = 18000 the turbulent production $\langle P_t \rangle$ in the cavity varies in the range of -0.0238 to 0.0567, but in the statistical symmetry plane the maximum value in the range of 0.03 to 0.045 occurs near the four corners. As the Re increases the region of highest $\langle P_t \rangle$ becomes narrower and the inner core of very low turbulent production $\langle P_t \rangle$ becomes larger. For Re = 18000 negative value of $\langle P_t \rangle$ of -0.004 occurs in the inner part of boundary layer of the ver-

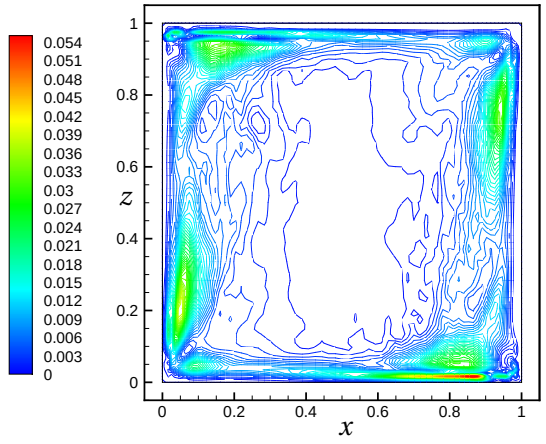

(a) Re = 12000. (In the domain $-1.14\times10^{-2} \le \langle P_t \rangle \le 1.21\times10^{-1}$)[13]

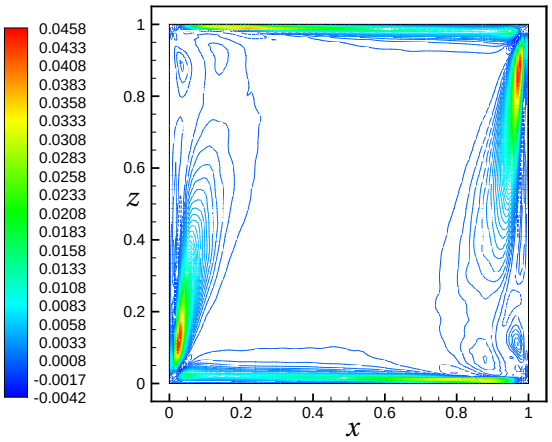

(b) Re = 18000 (In the domain $-2.38\times10^{-2} \le \langle P_t \rangle \le 5.67\times10^{-2}$)

Figure 6: The comparison of average turbulent production $\langle P_t \rangle$ at statistical symmetry plane ($y = 0.5$).

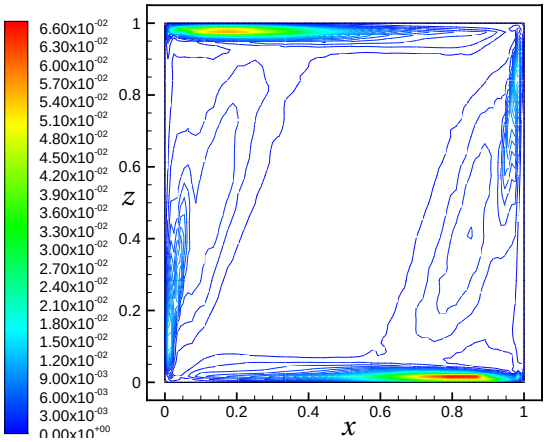

(a) Re = 12000 (In the domain $0 \le \langle \varepsilon \rangle \le 6.67\times10^{-2}$)

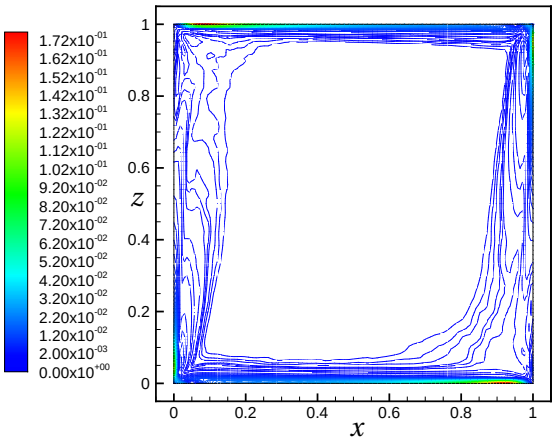

(b) Re = 18000 (In the domain $0 \le \langle \varepsilon \rangle \le 1.91\times10^{-1}$)

Figure 7: The comparison of averaged turbulent dissipation rate $\langle \varepsilon \rangle$ at statistical symmetry plane ($y = 0.5$).

tical wall jet.

The average turbulent energy dissipation rate $\langle \varepsilon \rangle$ is calculated by the Eq. 20 [2], where ω_i is the magnitude of vorticity.

$$\langle \varepsilon \rangle = \frac{1}{\mathrm{Re}} \left[\langle \omega_i \omega_i \rangle + 2 \frac{\partial^2 \langle \overline{u}_i \overline{u}_j \rangle}{\partial x_i \partial x_j} \right] \tag{20}$$

In Fig. 7 the highest average turbulent energy dissipation rate $\langle \varepsilon \rangle$ of 0.066 for Re = 12000 and of 0.172 for Re = 18000 occurs in the corner regions where the vertical wall jets hit the top and bottom moving lid. Another high values of $\langle \varepsilon \rangle$ at 0.02 for Re=12000 and at 0.1 for Re=18000 occur at the vertical wall corner where the fluid driven by the top and bottom moving lid impinges. In the central core region the turbulent energy dissipation rate $\langle \varepsilon \rangle$ is almost zero.

Two Dimensional Flow Profiles On $y-z$ Plane

The clockwise main recirculating flow pattern in the $x-z$ plane accompanied by corner eddies dominates the flow as described in the previous section. The three-dimensional flow pattern will be revealed in this section by studying the flow in the $y-z$ planes at three locations of $x = 0.81$ (near to the right-side wall), 0.5 (at the middle of the cavity) and 0.19 (near to the left-side wall) as shown in the Fig. 8. In Fig. 9, on vertical plane x=0.81 near to the right-side wall, the velocity vectors show that near to the top moving lid the magnitude of vertical w-component of velocity is very low due to the flow in this region be-

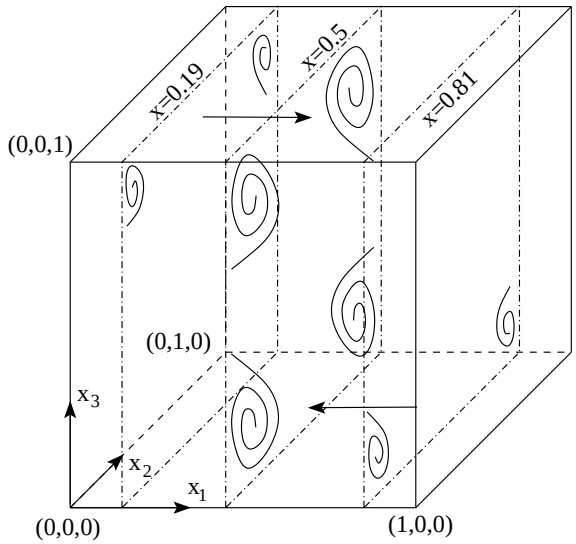

Figure 8: Vortices in the y-z planes [$(x_1, x_2, x_3) \equiv (x, y, z)$].

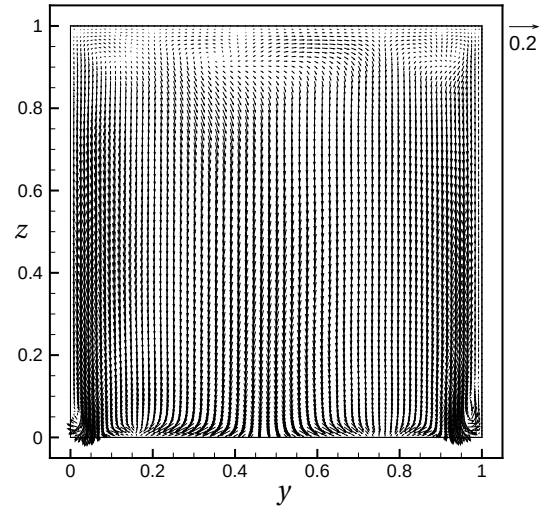

(a) Near the right wall of the cavity at $x = 0.81$ for Re = 12000.

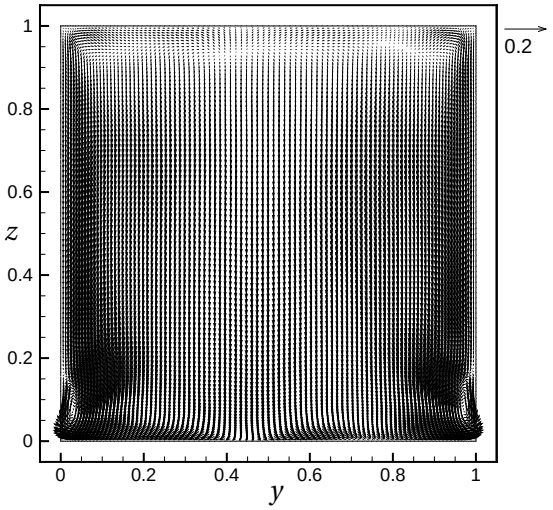

(b) Near the right wall of the cavity at x = 0.81 for Re = 18000.

Figure 9: Velocity vector field and vortices in the y-z plane at x=0.81

ing driven by the moving top lid. As flow continues in the downward direction the w-component of velocity increases by the affect of wall jet present in the right-side wall. It is noted here that after some distance from the top lid, the magnitude of vertical w-component of velocity is comparatively higher near to the front wall and near to the rear wall in the Fig. 9 and this flow separates from the front and rear wall resulting in the formation of eddy very near the bottom lid. It shows that from the impingement of fluid into the right-side wall near the top lid to the bottom of the right-side wall, some amount of fluid separates from the wall jet and it travels sideways towards the front and back walls along the transverse axis (y-axis), but when it comes with contact of the affect of core flow it changes the direction towards the bottom lid. Similar flow behavior with two eddies forming very near the top lid is seen for the vertical plane x=0.19 near the left-side wall, but is not presented in this paper for brevity. The nature of flow remains the same when the Reynolds number is increased from 12000 to 18000 but the strength of the eddies increases with Reynolds number.

These four eddies in the $y-z$ plane (two at the top in x=0.19 plane and two at the bottom in x=0.81 plane) travels along the direction of main flow driven by the top and bottom moving lids, and their fate are shown in the midplane in the Fig. 8 and Fig 10. The size of these eddies increases as it travels in the flow direction along the top and bottom moving lid and completely disappear at the far end. It is noted here that the vorticity vector at the center of these eddies are having dominant component in the x-direction and as the eddy travels in the flow direction and grows in size this component of vorticity decreases.

Turbulence Characteristics In Three Dimensional Region

Fig. 11 has been plotted for the region where turbulent production $\langle P_t \rangle$ is more than 0.8 % of its maximum value $\langle P_t \rangle_{max}$. This is the region where exchange of energy from mean flow to turbulent eddies take place. The turbulent production is high in the region very close to the top and bottom moving lids, and also in the corner region of the vertical wall where the fluid driven by the top and bottom

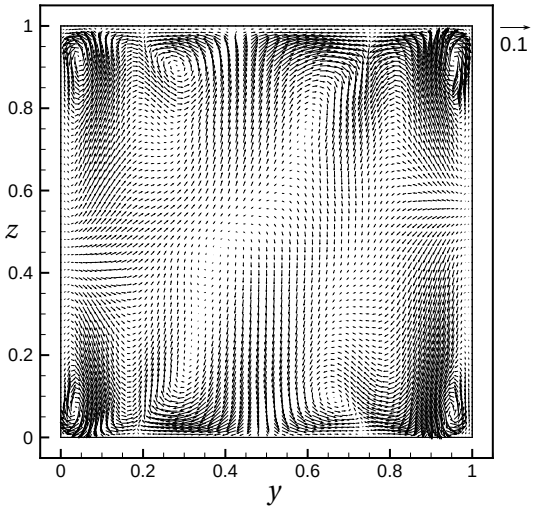

(a) At middle of the cavity at x = 0.5 for Re = 12000.

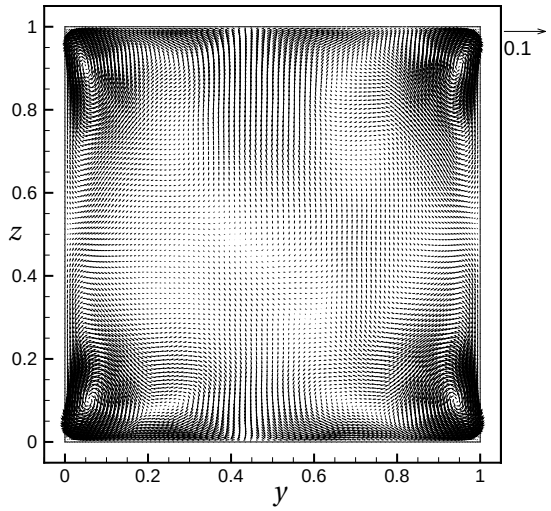

(b) At middle of the cavity at x = 0.5 for Re = 18000.

Figure 10: Velocity vector field and vortices in the y-z plane at x=0.5

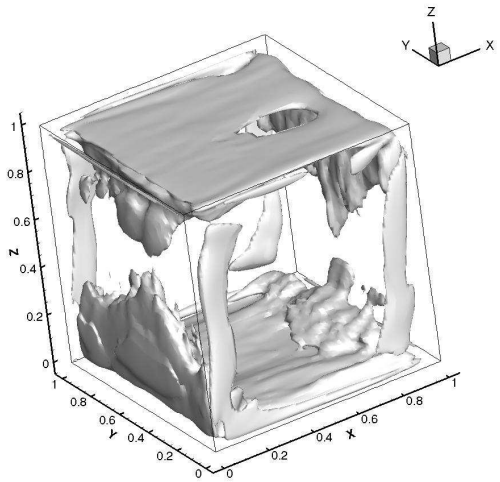

(a) At Re = 12000.

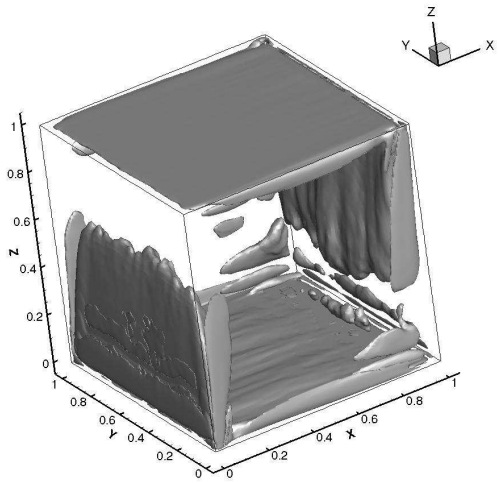

(b) At Re = 18000.

Figure 11: The region of cavity where $|\langle P_t\rangle|/|\langle P_t\rangle_{max}| > 0.008$.

moving lid impinges. In other regions there is almost no turbulent production. As the Reynolds number increases from 12000 to 18000, the region with more than 0.8% of $\langle P_t\rangle_{max}$ becomes thinner and the central region of almost no turbulent production increases.

The region of cavity where the average turbulent energy dissipation rate is more than 10% of its maximum value $\langle\varepsilon\rangle_{max}$, has been plotted in the Fig. 12. In this region eddies break down into smaller eddies; and it shows indirectly the zones of localization of small-scale structures. As the value of $\langle\varepsilon\rangle$ increases, more small-scale structures participate in the dissipation of turbulent energy. It can be noted here that regions where the recirculating fluid hits the solid wall (moving or stationary), is dissipating more turbulent energies compared to other places in the cavity. As the Reynolds number increases from 12000 to 18000, the region with more than 10% of $\langle\epsilon\rangle_{max}$ becomes thinner.

CONCLUSION

The Large Eddy Simulation with Dynamic Smagorinsky Model (LES-DSM) of two sided cubic lid-driven cavity with lids moving in anti-parallel direction at high Reynolds number 12,000 and 18000 have been presented.

Two corner eddies in the $x-z$ plane are found at the mid plane y = 0.5 in the case of two sided lid-driven

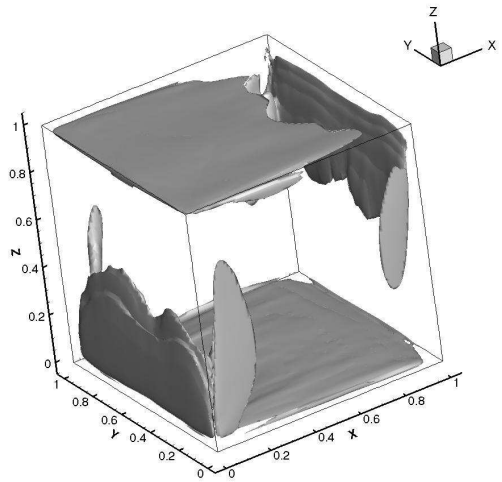

(a) Re = 12000.

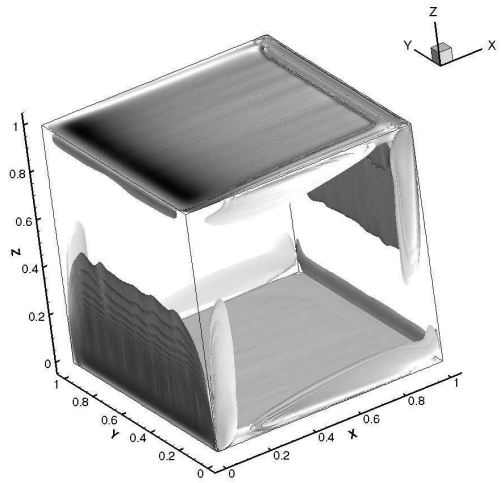

(b) Re = 18000.

Figure 12: The region of cavity where $|\langle\varepsilon\rangle|/|\langle\varepsilon\rangle_{max}| > 0.1$.

cavity with anti-parallel motion of opposite walls. The size of the two corner eddy in the $x-z$ plane is reduced as the Reynolds number increases. These eddies in the $y-z$ plane rotating in opposite directions travels along the flow driven by the moving lids while the size of eddies increases and x-component of vorticity decreases until it completely disappears.

The zone of high turbulence production and high dissipation of turbulent kinetic energy are identified. These zones of high turbulence production, high dissipation of turbulent kinetic energy become thinner with the increase of Reynolds number. There is a large central recirculating region with very low production and dissipation of turbulence.

REFERENCES

[1] P. N. Shankar and M. D. Deshpande. Fluid mechanics in the driven cavity. *Annu. Rev. Fluid Mech.*, 32:93–136, 2000.

[2] Roland Bouffanais, Michel O. Deville, and Emmanuel Leriche. Large-eddy simulation of the flow in a lid-driven cubical cavity. *Phys. Fluids*, 19:055108, 2007.

[3] E. Leriche and S. Gavrilakis. Direct numerical simulation of the flow in a lid-driven cubical cavity. *Phys. Fluids*, 12:1363–1376, 2000.

[4] Emmanuel Leriche. Direct numerical simulation in a lid-driven cubical cavity at high reynolds number by a chebyshev spectral method. *J. Sci. Comput.*, 27: 335–345, 2006.

[5] B. Ben Beya and T. Lili. Three-dimensional incompressible flow in a two-sided non-facing lid-driven cubical cavity. *C. R. Mecanique*, 336:863–872, 2008.

[6] F. Oueslati, B. Ben Beya, and T. Lili. Aspect ratio effects on three-dimensional incompressible flow in a two-sided non-facing lid-driven parallelepiped cavity. *C. R. Mecanique*, 339:655–665, 2011.

[7] Devendra Kumar Patel, Manab Kumar Das, and Subhransu Roy. LES of incompressible turbulent flow inside a cubical cavity driven by two parallel lids moving in opposite direction. *International Journal of Heat and Mass Transfer*, 67:1039 – 1053, 2013.

[8] J. Smagorinsky. General circulation experiments with the primitive equations i. the basic experiment. *Mon. Weather Rev.*, 91(3):99–164, 1963.

[9] Massimo Germano, Ugo Piomelli, Parviz Moin, and William H. Cabot. A dynamic subgrid-scale eddy viscosity model. *Phys. Fluids A, Fluid Dyn.*, 3:1760–1765, 1991.

[10] D. K. Lilly. A proposed modification of the germano subgrid-scale closure method. *Phys. Fluids A, Fluid Dyn.*, 4:633–635, 1992.

[11] G. Hoffmann and C. Benocci. Numerical simulation of spatially-developing planar jets, agard-cp 551. *Proceeding of the 74th Fluid Dynamics Symposium at Greece*, pages 26.1–26.2, 1994.

[12] U. Piomelli and J. Liu. Large-eddy simulation of rotating channel flows using a localized dynamic model. *Phys. Fluids*, 7:839–848, 1995.

[13] Devendra Kumar Patel, Manab Kumar Das, and Subhransu Roy. LES of turbulent flow in a cubical cavity with two parallel lids moving in opposite direction. *International Journal of Heat and Mass Transfer*, 72:37 – 49, 2014.